4 Interferometry

Density changes in the fluid can be monitored by the use of interferometry because they affect the optical path in the arm of the interferometer passing through the fluid. In this chapter we discuss the conversion of an interferogram to a density distribution and we suggest a procedure for the determination of the thermal diffusivity by analysis of interferograms.

4.1 Interferograms

Interference results from the recombination of the two parts of a beam of light which is divided by the beamsplitter in the IFU (see fig. 3.4). The actual interference order at a location in an interferogram depends on the optical path lengths of both parts. In this section, we present the basic interference order equation and our method to determine the interference order in interferograms.

4.1.1 Interference order

An example of an interferogram when the fluid is homogeneous is displayed in fig. 4.1. The grey, horizontal belt in the interferogram is where the fluid meets the (transparent) quartz substrate, i.e. the heater. The area below it depicts the fluid. The spot in the centre of the picture originates from the narrow laser beam and is not part of the interferogram. The z-axis we chose along the direction of gravity in earth-bound experiments and the y-axis perpendicular to it in the plane of the interferogram. The x-axis is along the optical axis, perpendicular to the plane of the interferogram.

At a location (y, z) in the interferogram, the interference order $k(y, z)$ is determined by the difference in optical path length between two rays that meet at (y, z), of which one leads through the fluid and the other follows the arm of the interferometer towards the IFU-mirror (see fig. 3.4). When the fluid is homogeneous in every (y, z)-plane, the path of the ray through the fluid is at all times parallel to the heater, along the optical axis. Changes in the density of the fluid along the

path of such a ray correspond to an average change in refractive index $\Delta n(y,z)$ which, consequently, changes the optical path difference at (y,z) in the interferogram. The corresponding change in interference order, $\Delta k(y,z)$, then relates to the laser light wavelength, Λ, the path length of light in the sample, L, and $\Delta n(y,z)$ according to:

$$\Delta k(y,z) = \frac{L}{\Lambda}\Delta n(y,z)\,. \tag{4.1}$$

Figure 4.1 An example of an interferogram.

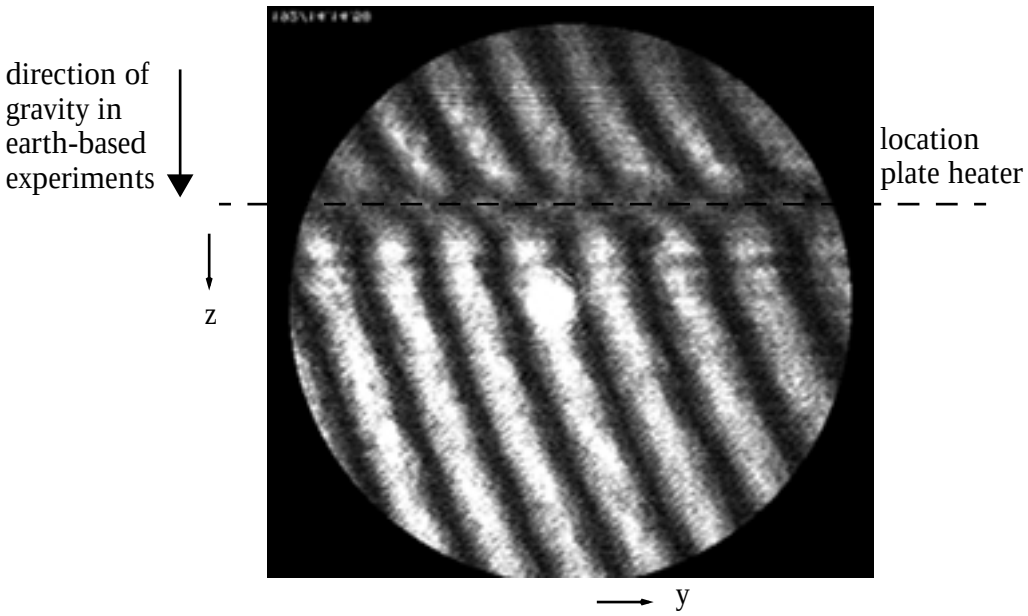

4.1.2 Interferogram analysis

When the fluid is homogeneous, the optical path of the arm through the fluid is equal for all positions (y,z). In this case the fringes in the interferogram are straight and the number and their angle w.r.t. an arbitrary axis are determined by the tilt in the tilt mirror in the other interferometer arm. Thus, the fringes are equidistant as is displayed in fig. 4.1. Therefore, $k(y)$ for a specific z takes on the form of a periodic function. In the small region of the fluid that is monitored by interferometry, generally the density of the fluid is just a function of z; e.g. upon heating with the gold plate, in a plane parallel to the heater the fluid remains homogeneous. Therefore, at z_1 after a time Δt, the change in interference order $\Delta k(y,z_1)$ is equal for all y, and $k(y,z_1)+\Delta k(y,z_1)$ remains a periodic function of which only the phase differs from that of $k(y,z_1)$. By means of Fourier transformation of $k(y,z_1)$, it is possible to determine accurately the period and the phase of the leading component of this periodic function and, ergo, a difference in interference order.

The determination of order differences by means of Fourier transformation at many z-positions leads to a $\Delta k(z)$ of which the values do not exceed an order difference of 0.5; phase differences between two (periodically equal) functions are determined within a multiple of 2π. Therefore, in order to find the underlying $\Delta n(z)$, the $\Delta k(z)$ needs to be “unwrapped”. Usually, this unwrapping is accomplished unambiguously. However, in some cases it has proved to be impossible to perform this unwrapping to a satisfactory level. Unfortunately, these datapoints had to be discarded.

4.2 Inhomogeneous density fields

In eq. (4.1), the interference order Δk is independent of the x-position of the observation plane of the interferogram since the starting point is that the light travels along a straight path through the fluid. However, near the heater, density gradients will arise upon heating resulting into an inhomogeneous refractive index field in which light is deviated according to Snell's law. Fortunately, in the bulk of the fluid the light is not deviated since the bulk response to local heating generally is homogeneous (PE) and the gradients in the boundary layers at the window and mirror merely affect the optical path length but not the direction of the propagating light. To a large extent, the effect of the deviation of the light rays may be dealt with conveniently by proper focusing of the optical system [37]. In this section we review the paths of light rays through inhomogeneous fields and proper focusing.

4.2.1 Deviation of Light Rays

It is implicitly assumed that geometrical optics can be applied to describe the propagation of light through the inhomogeneous sample. The condition [64] for this is that the relative change of the refractive index over one wavelength is small, hence

$$\frac{1}{n}\frac{dn}{dz} << \frac{1}{\Lambda}. \tag{4.2}$$

Due to the density gradient following linear heating, light rays passing through the sample will meet with higher density and hence with higher values of the refractive index, the further away from the heater they pass through the sample. Therefore the rays will be bend away from the heater. This bending is governed by the generalization of Snell's law, which states that for one ray

$$n(z)\cos\vartheta(z) = \text{constant} \tag{4.3}$$

where $\vartheta(z)$ is the angle between the ray and the horizontal plane as illustrated in fig. 4.2.

Figure 4.2 Geometry of a light ray passing through an optically inhomogeneous sample.

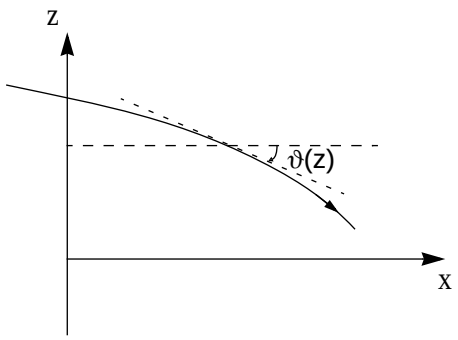

In order to obtain a relation $z(x)$ for the path of the ray, eq. (4.3) has to be differentiated with respect to z. Since $\frac{dz}{dx} = \tan\vartheta$, this yields

$$\frac{1}{n}\frac{dn}{dz} = \frac{d\vartheta}{dx} \tag{4.4}$$

And, $z(x)$ is determined by the differential equation

$$\frac{d^2z}{dx^2} = \frac{d}{dx}\tan\vartheta = \left\{1 + \left(\frac{dz}{dx}\right)^2\right\}\frac{d\vartheta}{dx} \tag{4.5}$$

As an example, we present in fig. 4.3 the light paths for beams entering a sample of carbondioxide, subject to the earth's gravitational field. They are reprinted from ref. [72]. We see that, much as expected, the light rays are curved stronger in areas of higher gradients. Very close to CP, where the fluid is highly stratified in a small region, this leads to the phenomenon of ray crossing.

Figure 4.3 Gravity induced deviation of a beam of light in a critical sample at various temperatures; the dashed line indicates the level at which $\rho=\rho_c$ (the meniscus).

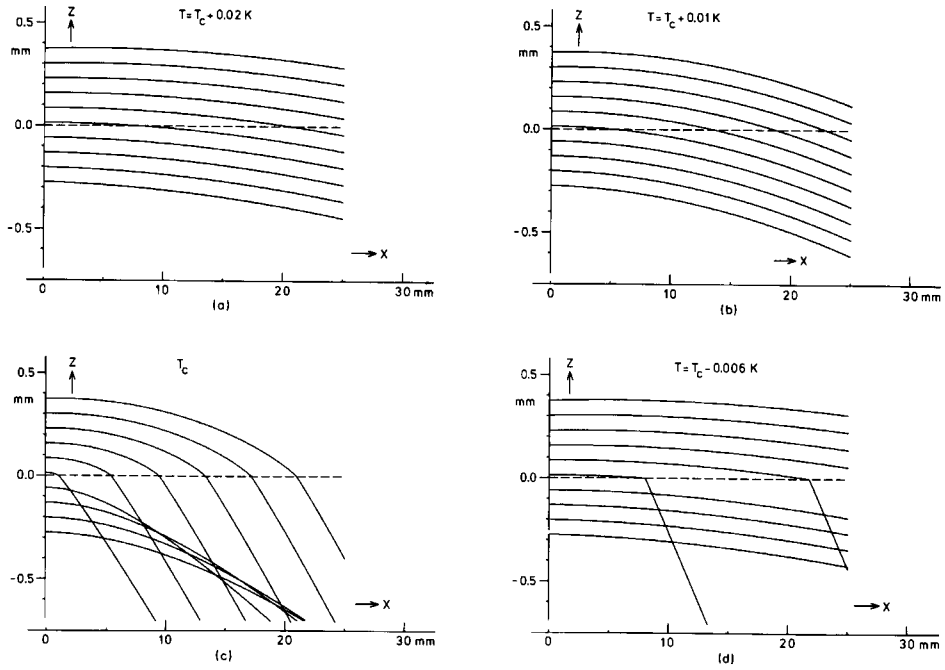

4.2.2 The parabolic approximation

When the fluid is heated by the gold layer, light rays will meet with higher density the further away from the heater they pass through the sample. Therefore the rays will bend away from the heater as illustrated in fig. 4.4. Also indicated are the path of the undeviated ray and the virtual straight path inside the fluid deduced from the exit angle ϑ of the light ray. In the interferometry chamber, through the sample, the light overpasses a distance D (= 16 mm) twice as the beam is reflected by the mirror, so that $L = 2D$. The mirror position is represented in fig. 4.4 by the dashed line in the middle of the heater to account for this double passing.

Figure 4.4 Schematic representation of the path of a ray through the sample.

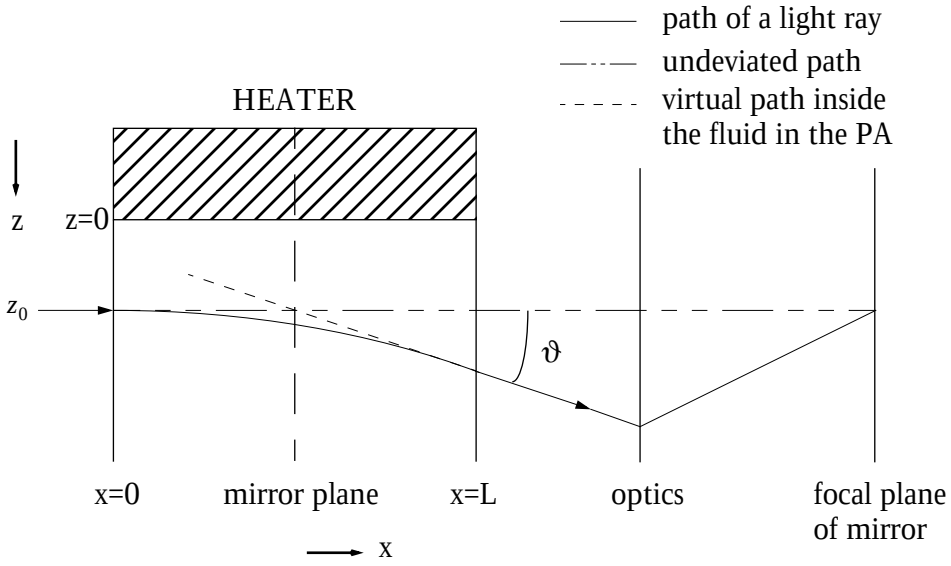

In order to find the actual path of the ray we turn to eq. (4.5) by which the path is determined in an inhomogeneous field. Ignoring higher order terms, we find for a ray entering parallel to the heater at z_0:

$$z - z_0 = \left(\frac{1}{n}\frac{dn}{dz}\right)_{z_0} \frac{1}{2}x^2 + \left(\frac{1}{n^2}\frac{dn}{dz}\frac{d^2n}{dz^2}\right)_{z_0} \frac{1}{24}x^4 + \ldots . \tag{4.6}$$

When we assume that the gradient of the refractive index is constant along the path of the ray, the second term on the right hand side of eq. (4.6) vanishes. In this approximation the light path describes a parabola and, therefore, often is called the parabolic approximation (PA).

When rays are deflected, the interferograms no longer can be described in terms of plane wavefronts and imaging effects become important. Under these conditions $\Delta k(y, z)$ is no longer independent of x. The corrections to be made to eq. (4.1) to account for refraction by the fluid are given by Hauf and Grigull [73] for the case that the detection plane is placed in the focal plane of the middle of the sample (in our configuration the mirror). In “The parabolic approximation” on page 105 (section E.1), it is calculated under which experimental circumstances the PA is valid.

In the PA the intersection of the undeviated path and the virtual path lies halfway the sample, i.e. at the mirror, and, therefore, focusing of the detection plane onto the mirror means that a ray entering at a height z_0 will meet the detection plane at the same height as the undeviated ray would. The advantage of focusing this way is that at all times the same correspondence exists between the entrance location of a light ray and its position in the interferogram, independent of the deflection angle. Furthermore, the image of the fluid adjoins the image of the heater resulting in a maximum resolution without overlap between the two. However, a correction to eq. (4.1) is necessary.

By the curvature of the light ray the geometrical path inside the fluid is increased. An essential property of image formation by an optical system is that there exists for each point, within certain limits, an image point such that the optical path is the same by any of the possible routes through the optical system. This means that it is possible to trace both the real light ray as well as the unde-

viated ray to the same point so that both the optical paths are equal. Imaging this way enables the use of eq. (4.1) without corrections. Both Becker [37] and Svensson [74] found that, in the PA, the increase in optical path is compensated for by focusing on $x = 2/3L$. Still, focusing in this way introduces a dependence on time of the imaged position. For more accurate approximations of the light paths no plane exists for which the interference order in the entire interferogram is described by eq. (4.1).

4.2.3 Influence of the cold walls

The temperature profile at the heater is generally given by eq. (A.23). In section 2.2.3 it is argued that the deviation from uniformity may be approximated by the constant pressure result of eq. (2.38). However, near the entrance window and the mirror the profile is disturbed by the temperature gradients that arise near these 'cold' boundaries. In order to determine the effect of this on the interferogram we solved numerically the light paths through the fluid for a two-dimensional density field. An exact calculation of the density field in two dimensions both near the heater as well as near these boundaries proves to be a very complicated task. Since we expect the disturbance of the general profile perpendicular to the heater to be only a small side effect, we start with an approximated density field. For this approximation we turn to the temperature profile at the 'cold' boundaries far from the heater, i.e. eq. (A.14). The effect of the bulk temperature change on the profile near the 'cold' boundaries we extrapolate towards the heater according to

$$\hat{T}(x, z, t) = \{\hat{T}_{f,p}(z, t) + \hat{T}_b(t)\}\frac{\hat{T}_b(t) - \delta T(x, t)}{\hat{T}_b(t)}, \tag{4.7}$$

where $\delta T(x, t)$ is determined by eq. (A.14). The corresponding density field follows from this temperature field simply by the application of eq. (2.46). The outcome of the numerical simulations is that for situations where the parabolic approximation is valid, the effect of the 'cold' boundaries on the interferogram is negligible.

4.3 Shadow evaluation

In interferometry, usually, the components of the superposition are supposed to be parallel beams, so that imaging effects are not important. However, from the previous sections it has become clear that, when dealing with inhomogeneous fluids, proper focusing is of paramount importance. In the laboratory equipment we were able to arrange the optics to our requirements, but this was not possible for the CPF. In the actual CPF configuration, for our SCU neither the CCD nor the photocamera optical systems are focused in either of the two ways suggested in section 4.2.2, i.e. on the mirror or on $x = 2/3L$. Consequently, for the region close to the heater, where $dn/dz \neq 0$, serious corrections to eq. (4.1) are required; these involve the interference order as well as the image position. Unfortunately, this makes the 'image restauration' unnecessary complex and greatly reduces the accuracy with which the $\rho(z)$-profile can be determined. The determination of D_T from $\rho(z)$, based on eq. (2.38) therefore becomes unfeasible and the development of an alternative procedure is required.

4.3.1 The appearance of a shadow

In the PA, focusing onto the middle of the sample, i.e. the mirror, results in an obvious relation between the locations in the fluid and in the interferogram; the image of the fluid adjoins the image of the heater so that the space-coordinates just are scaled by the magnification of the optical system. When the optical system is focused differently, or, analogously, when the film of the camera is positioned at a location different from the image plane of the mirror, upon heating with the gold-plate a 'shadow' will arise in the interferogram between heater and fluid. In order to clarify this phenomenon, a schematic representation of the path of a ray in the PA passing through the sample entering at position z_0 parallel to the heater is displayed in fig. 4.5.

Figure 4.5 Schematic representation of the path of rays through the sample and the optics to the image plane and camera-film.

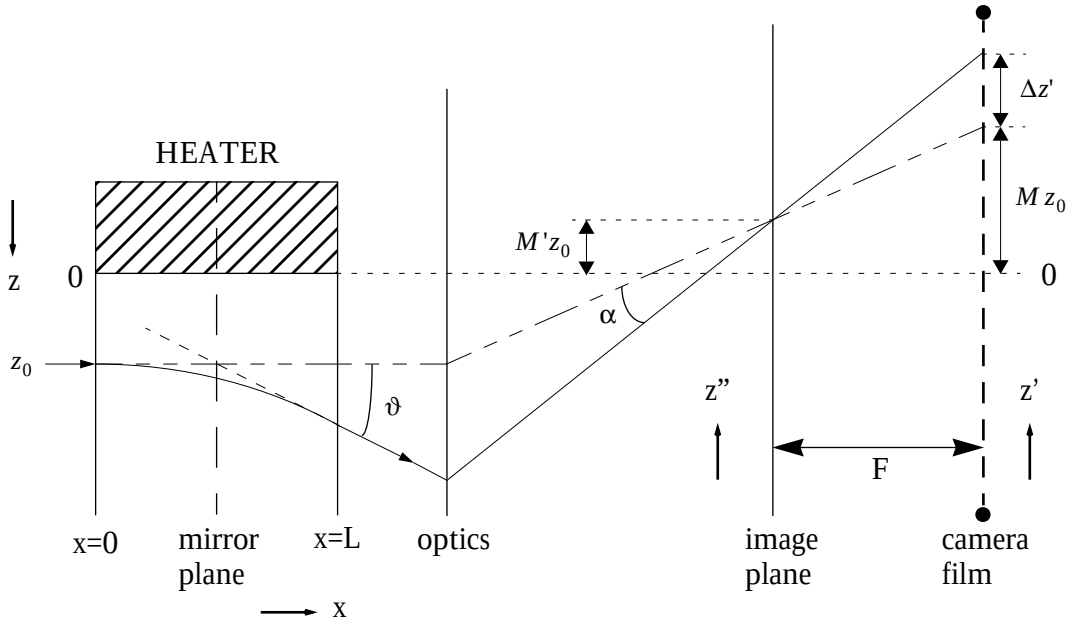

The ray entering the interferometry chamber parallel to the heater will exit under an angle ϑ w.r.t. the heater. From the previous section 4.2.2, in the PA a ray entering at height z_0 leaves the cell seemingly coming from the mirror at this height z_0. When M' is the linear magnification of the optics, a ray entering at height z will meet the image plane at position z'' according to

$$z'' = M'z . \tag{4.8}$$

When the camera-film is positioned at a distance F from this image plane, the ray will meet the film plane differently w.r.t. to a ray undeflected by the sample as indicated in fig. 4.5. When N is the angular magnification of the optics so that the (exit) angle ϑ is magnified to α through

$$\alpha = N\vartheta , \tag{4.9}$$

the deviation $\Delta z'$ w.r.t. the undeflected ray in the film plane is:

$$\Delta z' = F\alpha = FN\vartheta . \tag{4.10}$$

Thus, accounting for the magnification M in the film plane, in the PA a ray entering at position z will be detected at a position z' according to

$$z' = Mz + FN\vartheta . \tag{4.11}$$

Since all rays will bend away from the heater, locating the film at a position different from the image plane of the mirror causes a part of the interferogram to be unexposed by the beam passing through the fluid. No interference will happen in this region leading to what appears to be a 'shadow' adjacent to the position where the heater is projected $(z' = 0)$. An example of such an interferogram is displayed in fig. 4.6.

Figure 4.6 An example of a shadow adjacent to the heater.

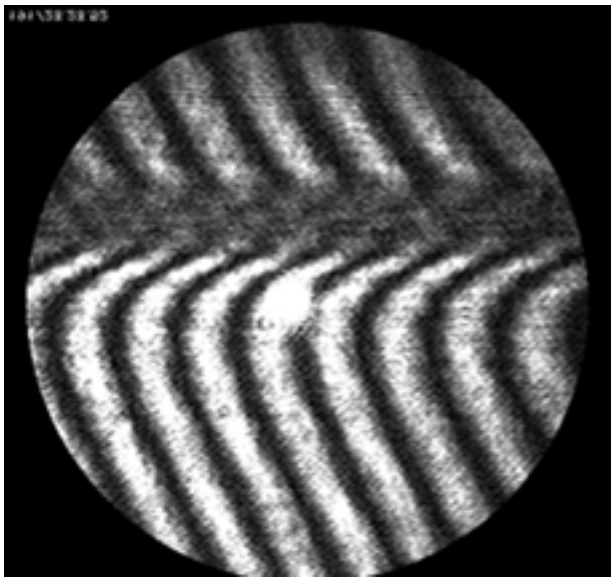

In order to relate the imaging properties to the refractive index (or density-) gradients in the sample, we define an average gradient along a ray g_n by

$$g_n \equiv \frac{1}{L}\int_0^L \frac{1}{n}\frac{dn}{dz}dx , \tag{4.12}$$

where L is the total length of the ray through the sample. Ignoring terms beyond x^4 in eq. (4.6), we find for a ray entering parallel to the heater at z_0:

$$g_n = \left(\frac{1}{n}\frac{dn}{dz}\right)_{z_0}\left[1 + \frac{L^2}{6}\left(\frac{1}{n}\frac{d^2 n}{dz^2}\right)_{z_0}\right], \tag{4.13}$$

Note that in the parabolic approximation

$$g_n = \left(\frac{1}{n}\frac{dn}{dz}\right)_{z_0} . \tag{4.14}$$

According to eq. (4.4), the angle ϑ then is

$$\vartheta = Lg_n . \tag{4.15}$$

The real path of a ray entering at z_0 may leave the cell seemingly coming from the mirror at a different height than z_0 (see also section E.1.2). To account for this difference Δz_m at the mirror, we rewrite eq. (4.11) to the general relation describing the detection in the film plane of a ray entering parallel to the heater:

$$z' = M\,[z + \Delta z_m(z,t)] + FNLg_n(z,t)\,. \tag{4.16}$$

Ignoring terms beyond x^4 in eq. (4.6), we find for a ray entering parallel to the heater at z_0:

$$\Delta z_m = -\frac{L^4}{24}\left(\frac{1}{n^2}\frac{dn}{dz}\frac{d^2n}{dz^2}\right)_{z_0}\,. \tag{4.17}$$

Not surprisingly, in the parabolic approximation $\Delta z_m = 0$.

4.3.2 An alternative procedure

The density field following heating by the gold-plate will have a gradient high at the heater $(z = 0)$ and decreasing with increasing distance from the heater. Figure 4.7 shows two types of deviations (I and II) w.r.t. a parallel beam as a result of this kind of density field. In this figure, the detected position (z') at the film plane is displayed versus the entrance distance (z) to the heater. When the deviations are such that $z_1' < z_2'$ for $z1 < z2$, the size of the 'shadow' is determined by the detector position of the ray entering at $z = 0$. This we will refer to as a type I deviation. For a ray entering at position $z = 0$, the detector position z' is just a function of g_n. The refractive index gradient is proportional to the density gradient, which at $z = 0$ is proportional to the heat-flux from the gold-plate into the fluid. This leads to the conclusion that for a constant heat-flux, in the PA the imaged position $z'(z = 0)$ is a constant in time. Thus, a type I deviation results in a constant size of the 'shadow'.

Figure 4.7 Deviations w.r.t. to a parallel beam of a beam passing through a density field following heating at one side.

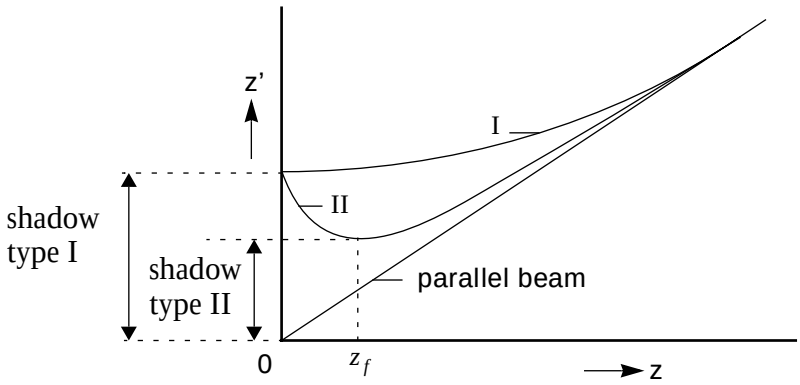

However, for relatively small times, the density gradient near the heater rapidly decreases with increasing distance from the heater. Just as in the case of the strong stratification in a small region very close to CP, this leads to the phenomenon of ray crossing (see fig. 4.3). The ray entering at $z = 0$ will cross other rays and will meet the film plane further away from the apparent heater than some other rays and, consequently, the size of the 'shadow' is determined by another ray. This sit-

uation we call a type II deviation. In type II, the size of the 'shadow' is determined by a ray entering at position $z = z_f$ for which:

$$\frac{dz'}{dz} = 0. \tag{4.18}$$

Utilizing eq. (4.16), condition (4.18) reads

$$\frac{dg_n}{dz} = -\frac{M}{FNL}\left[1 + \frac{d}{dz}(\Delta z_m)\right]. \tag{4.19}$$

When the parabolic approximation is valid, i.e. g_n is described by eq. (4.14) and $\Delta z_m = 0$, eq. (4.19) implies that (for type II) the size of the 'shadow' is determined by a ray entering at position z_f for which

$$\left(\frac{d^2\rho}{dz^2}\right)_{z=z_f} = -\frac{Mn}{FNL}\frac{d\rho}{dn}, \tag{4.20}$$

where $\frac{1}{n}\frac{dn}{d\rho}$ is assumed constant along the path of the ray. Combining eq (2.38), that describes the temperature deviation from uniformity, and eq. (2.57), that relates the temperature and the density, leads to:

$$\left(\frac{d\rho}{dz}\right)_{z=z_f} = \frac{\rho\alpha_P}{\lambda}\frac{q_f}{S_h}\operatorname{erfc}\left(\frac{z_f}{2\sqrt{D_T t}}\right) \tag{4.21}$$

and

$$\left(\frac{d^2\rho}{dz^2}\right)_{z=z_f} = -\frac{K_1}{\sqrt{\pi D_T t}}\exp\left(-\frac{z_f^2}{4D_T t}\right), \tag{4.22}$$

where

$$K_1 \equiv \frac{\rho\alpha_P}{\lambda}\frac{q_f}{S_h}. \tag{4.23}$$

With eq. (4.20) z_f is found:

$$z_f^2 = -4D_T t \ln\left(\frac{K_2}{K_1}\sqrt{\pi D_T t}\right), \tag{4.24}$$

where

$$K_2 \equiv \frac{Mn}{FNL}\frac{d\rho}{dn}. \tag{4.25}$$

After substituting z_f from eq. (4.24) into eq. (4.16), again in the PA and utilizing eq. (4.21), some algebra leads to:

$$z_f' = M Z_0\left\{\frac{2}{\sqrt{\pi}}\zeta\exp(-\zeta^2) + \operatorname{erfc}(\zeta)\right\}, \tag{4.26}$$

where

$$\zeta^2 \equiv -\ln(t/t_m)/2\,, \tag{4.27}$$

$$t_m \equiv \frac{Z_0^2}{\pi D_T} \tag{4.28}$$

and

$$Z_0 \equiv \frac{K_1}{K_2} = \frac{q_f}{S_h}\frac{\rho\alpha_p}{\lambda}\frac{1}{n}\frac{dn}{d\rho}\frac{FNL}{M}\,. \tag{4.29}$$

Equation (4.26) gives the position in time of the shadow front upon heating with a constant heat flux in the PA. In an experiment, from the evolution of this shadow front the value of D_T may be determined (see section 6.4). In section E.1 we show that, generally, for heating times much smaller than t_m the PA can be used to describe accurately the shadow front development. Close to CP t_m is large so that, for realistic heating times, the PA is applicable. Furher away from CP, where t_m becomes of the order of realistic heating times, numerical inversion has been used to determine D_T.

To give an idea as to the values of Z_0 and t_m in the critical region of SF_6, in fig. 4.8 both are displayed versus the distance to T_c for a power density of 0.5 W/m^2 and the CPF optical layout for the CCD camera. The CPF optical layout is listed for both the CCD camera and the photocamera in Table E.1 on page 111. For this case, in fig. 4.9 z_f is displayed for 5 different temperatures in a wide range above T_c up to 100 seconds after the onset of heating. Each curve is labelled by its corresponding temperature difference from T_c.

Figure 4.8 Z_0 and t_m versus the distance to T_c for SF_6 and CPF-optics.

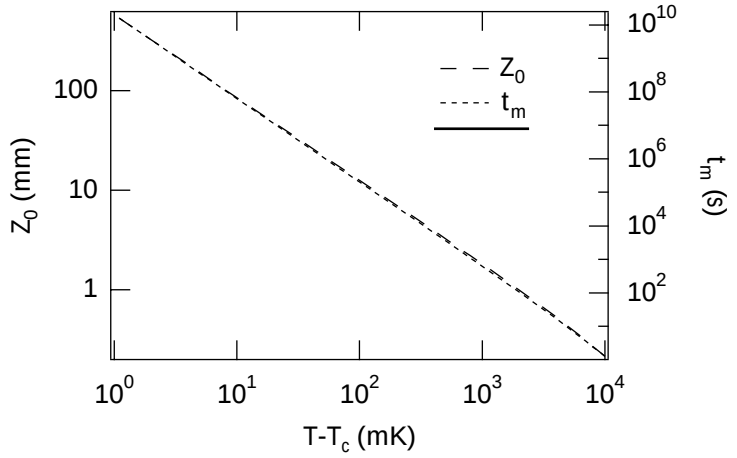

Figure 4.9 z_f in time for various temperatures.